Accepted Manuscript

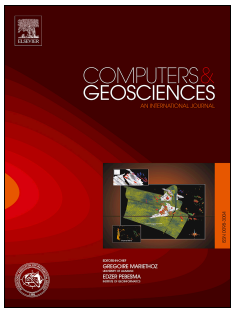

Finite-element time-domain modeling of electromagnetic data in general dispersive medium using adaptive Padé series

Hongzhu Cai, Xiangyun Hu, Bin Xiong, Michael S. Zhdanov

PII: S0098-3004(17)30007-9

DOI: 10.1016/j.cageo.2017.08.017

Reference: CAGEO 4014

To appear in: *Computers and Geosciences*

Received Date: 3 January 2017

Revised Date: 2 July 2017

Accepted Date: 29 August 2017

Please cite this article as: Cai, H., Hu, X., Xiong, B., Zhdanov, M.S., Finite-element time-domain modeling of electromagnetic data in general dispersive medium using adaptive Padé series, *Computers and Geosciences* (2017), doi: 10.1016/j.cageo.2017.08.017.

Finite-element time-domain modeling of electromagnetic data in general dispersive medium using adaptive Padé series

Hongzhu Cai[a,b], Xiangyun Hu[c], Bin Xiong[d,*], Michael S. Zhdanov[a,b,e]

[a] *Consortium for Electromagnetic Modeling and Inversion (CEMI), University of Utah, Salt Lake City, Utah, USA 84112*
[b] *TechnoImaging, Salt Lake City, UT 84107 USA*
[c] *China University of Geosciences, Institute of Geophysics and Geomatics, Wuhan, China*
[d] *College of Earth Sciences, Guilin University of Technology, Guilin, Guangxi, China 541004*
[e] *Moscow Institute of Physics and Technology, Moscow 141700, Russia*

Abstract

The induced polarization (IP) method has been widely used in geophysical exploration to identify the chargeable targets such as mineral deposits. The inversion of the IP data requires modeling the IP response of 3D dispersive conductive structures. We have developed an edge-based finite-element time-domain (FETD) modeling method to simulate the electromagnetic(EM) fields in 3D dispersive medium. We solve the vector Helmholtz equation for total electric field using the edge-based finite-element method with an unstructured tetrahedral mesh. We adopt the backward propagation Euler method, which is unconditionally stable, with semi-adaptive time stepping for the time domain discretization. We use the direct solver based on a sparse LU decomposition to solve the system of equations. We consider the Cole-Cole model in order to take into account the frequency-dependent conductivity dispersion. The Cole-Cole conductivity model in frequency domain is expanded using a truncated Padé series with adaptive selection of the center frequency of the series for early and late time. This approach can significantly increase the accuracy of FETD

*Corresponding author
Email addresses: caihongzhu@hotmail.com (Hongzhu Cai), xyhu@cug.edu.cn (Xiangyun Hu), hsiungbin@hotmail.com (Bin Xiong), michael.s.zhdanov@gmail.com (Michael S. Zhdanov)

modeling.

Keywords: Geophysical electromagnetics; Induced polarization; Finite-element time-domain; Padé series

1. Introduction

Time-domain electromagnetic (TEM) methods have been widely used to study subsurface conductive structures (Ward and Hohmann, 1988; Zhdanov, 2009). Compared to frequency-domain electromagnetic methods, the TEM method usually has better resolution and sensitivity to deep targets for typical transmitter-receiver configurations and broad time scales. The correct interpretation of the TEM data requires accurate forward modeling methods. There exist two major methods for solving this problem – one is based on the Fourier transform of the frequency-domain response to the time domain (e.g. Knight and Raiche, 1982; Everett and Edwards, 1993; Raiche, 1998; Mulder et al., 2007; Ralph-Uwe et al., 2008), and another exploits a direct discretization of the Maxwell's equation in both spatial and time domains (Wang and Hohmann, 1993; Commer and Newman, 2004; Maaø, 2007; Um et al., 2012; Jin, 2014).

Note that, the accuracy of Fourier transformation is affected significantly by the frequency sampling and the transformation methods, such as the choice of the digital filters (Li et al., 2016). The finite-difference time-domain (FDTD) methods have been used for modeling the electromagnetic response in time domain for decades (Yee, 1966).

We should note also that, in the framework of the finite-difference method, the complex geometries need to be approximated by a stair-cased model. It is well known that, these complications of finite-difference modeling, can be overcome by the finite-element approach. It has been demonstrated that the FETD method with unstructured spatial discretization can reduce the size of the problem dramatically (Um, 2011; Jin, 2014).

There are two major types of time discretization: 1) an explicit scheme, 2) an implicit scheme. The explicit scheme requires a small time step size to satisfy the

Courant stability condition (Wang and Hohmann, 1993; Um, 2011; Jin, 2014), which makes this approach computationally expensive for TEM modeling with time scale from a small fraction of a second to hundreds seconds (Zaslavsky et al., 2011). The implicit approach is unconditionally stable but it requires solving a linear system of equations with the matrix depending on the time step size. This problem can be addressed by adopting modern direct solvers, since the corresponding matrix needs to be decomposed only once for a fixed time step size (Um, 2011; Jin, 2014). We adopt the FETD scheme proposed by Um (2011) for solving the TEM modeling problem. We also update the time step, in an adaptive manner, to reduce the computational cost.

The conventional modeling of TEM data usually considers a non-dispersive medium, with frequency-independent conductivity. In the presence of IP effect, the conductivity becomes frequency dependent. It was shown by Pelton et al. (1978) that the conductivity relaxation model can be well represented by the Cole-Cole model. In this paper, we consider the dispersive conductive medium with the conductivity described by the Cole-Cole model. Zhdanov (2008) introduced a more general conductivity relaxation model based on the generalized effective-medium theory of IP (so called "GEMTIP" model). It was shown by Zhdanov (2008) that the GEMTIP model reduces to the Cole-Cole model in a special case of spherical inclusions within a homogeneous background model. We could update Cole-Cole model with GEMTIP model in our FETD modeling algorithm.

Frequency-dependent dispersion models need to be represented by a convolution of the electric field in the time domain. The convolution term can be introduced into Maxwell's equation through the fractional derivative with respect to time (Zaslavsky et al., 2011; Marchant et al., 2014). Solving such equations with convolution or fractional derivative terms requires the electric field at all previous stages (Zaslavsky et al., 2011), since either the convolution or the fractional derivative correspond to a global operator. Due to this problem, the TEM data with IP effect are rarely modeled directly in time domain.

The Padé series (Baker, 1996) can be used to avoid the fractional derivative

problem raised in modeling the EM field in dispersive medium (Weedon and Rappaport, 1997). The fractional differential equation can be transformed to the differential equation with integer order and further to be solved using numerical methods such as FDTD (Rekanos, 2010). Based on the work of Weedon and Rappaport (1997) and Rekanos (2010) for the FDTD method with the Padé approximation, Marchant et al. (2014) proposed a finite-volume time-domain method for simulating IP effect with the Cole-Cole model.

In all the publications cited above, in order to calculate the Padé coefficients, the Taylor series was implemented in the vicinity of one preselected center frequency. However, we will demonstrate that the accuracy of the corresponding Padé approximation depends significantly on the selected center frequency. In order to keep the same accuracy of the Padé approximation for different time moments, we propose selecting different central frequencies for early and late time moments. We call this approach the *adaptive Padé series.* We have implemented the FETD modeling with IP effect using this adaptive Padé approximation. Instead of using a Taylor expansion at the fixed point for calculating the Padé coefficients, we update the Padé coefficients adaptively during the FETD modeling process. This approach increases the accuracy of FETD modeling with IP effects.

2. Finite element time domain discretization of Maxwell's equation

The Maxwell's equations in time domain for the quasi-stationary EM field can be described as follows (Zhdanov, 2009; Jin, 2014):

$$\nabla \times \mathbf{E} = -\mu \frac{\partial \mathbf{H}}{\partial t}, \tag{1}$$

$$\nabla \times \mathbf{H} = \mathbf{j_e} + \mathbf{J_s}, \tag{2}$$

where $\mathbf{E}$ and $\mathbf{H}$ are electric and magnetic fields, $\mathbf{J_s}$ is the current density of the source, and $\mathbf{j_e}$ is the induction current density, described by the Ohm's law:

$$\mathbf{j_e} = \sigma \mathbf{E}. \tag{3}$$

In the last formula, σ is the electric conductivity. In a nondispersive medium, σ is time invariant.

We eliminate the magnetic field from the system of equations and obtain the diffusion equation for electric field:

$$\nabla \times \nabla \times \mathbf{E}(t) + \mu \frac{\partial \mathbf{j_e}(t)}{\partial t} = -\mu \frac{\partial \mathbf{J_s}(t)}{\partial t}. \tag{4}$$

We first consider that the conductivity is independent of time. Substituting equation (3) into (4), we obtain the following equation:

$$\nabla \times \nabla \times \mathbf{E}(t) + \mu\sigma \frac{\partial \mathbf{E}(t)}{\partial t} = -\mu \frac{\partial \mathbf{J_s}(t)}{\partial t}. \tag{5}$$

We consider the Dirichlet boundary conditions for equation (5), according to which the tangential component of electric field vanishes on the boundary of the modeling domain:

$$\mathbf{E}(t) \times \mathbf{v} = \mathbf{0}, \tag{6}$$

where $\mathbf{v}$ is the unit vector directs outside the surface of the modeling domain.

We can solve equation (5) using the edge-based finite element method (Jin, 2014) with an unstructured tetrahedral mesh. The electric field inside the tetrahedral element at any time t can be represented as the linear combination of the fields along the element edges at the same time moment:

$$\mathbf{E}^e(t) = \sum_{i=1}^{6} \mathbf{N}_i^e E_i^e(t). \tag{7}$$

We use the superscript e to emphasize the local electric field inside the element.

After applying the edge-based finite element analysis to (5), we arrive at a global system of equations as follows (Jin, 2014):

$$K\mathbf{E}(t) + \mu L \frac{\partial \mathbf{E}(t)}{\partial t} = -\mu T \frac{\partial \mathbf{J_s}(t)}{\partial t}, \tag{8}$$

where the stiffness matrices K and L are defined as follows:

$$K_{ij}^e = \int_{\Omega_e} (\nabla \times \mathbf{N}_i^e) \cdot \left(\nabla \times \mathbf{N}_j^e\right) dv, \tag{9}$$

$$L_{ij}^{e} = \int_{\Omega_e} \mathbf{N}_i^e \cdot (\sigma^e \mathbf{N}_j^e) dv, \tag{10}$$

and Ω_e indicates the domain for each element. K^e and L^e are the local stiffness matrices while K and L are the global stiffness matrices. Again, we use the superscript e to emphasize the local element (e.g. σ^e emphasize the conductivity for the local element). Note that the conductivity information has already been included in the stiffness matrix L as shown in (10). We also introduce another matrix T_{ij}^e similar as L_{ij}^e but without any conductivity information:

$$T_{ij}^{e} = \int_{\Omega_e} \mathbf{N}_i^e \cdot \mathbf{N}_j^e dv, \tag{11}$$

and the corresponding global matrix is denoted as T.

In this paper, we use the linear edge-based finite element method for simplicity and the stiffness matrix can be calculated efficiently using the analytical solution.

To approximate the time derivative of electric field in (8), we adopt the backward Euler approximation (Jin, 2014):

$$\frac{\partial \mathbf{E}(t)}{\partial t} \approx \frac{\mathbf{E}(t) - \mathbf{E}(t - \Delta t)}{\Delta t}, \tag{12}$$

where Δt is the time-step size. It can be shown that the backward Euler approximation is unconditionally stable, regardless of the choice of Δt. We have the similar equation for the current density:

$$\frac{\partial \mathbf{j_e}(t)}{\partial t} \approx \frac{\mathbf{j_e}(t) - \mathbf{j_e}(t - \Delta t)}{\Delta t}. \tag{13}$$

By substituting equation (12) into equation (8), we obtain:

$$K\mathbf{E}(t) + \frac{\mu}{\Delta t} L\mathbf{E}(t) = \frac{\mu}{\Delta t} L\mathbf{E}(t - \Delta t) - \mu T \frac{\partial \mathbf{J_s}(t)}{\partial t}. \tag{14}$$

From equation (14), we can see that, given proper initial and boundary conditions, we can calculate the electric field at time moment, t, from the values known in the previous time moment, $t - \Delta t$, and the source waveform, $\mathbf{J_s}(t)$.

Equation (14) can be written in a compact form as follows:

$$\mathbf{A}\mathbf{E}(t) = \mathbf{b}, \tag{15}$$

where:

$$\mathbf{A} = K + \frac{\mu}{\Delta t} L, \tag{16}$$

and

$$\mathbf{b} = \frac{\mu}{\Delta t} L\mathbf{E}(t - \Delta t) - \mu T \frac{\partial \mathbf{J_s}(t)}{\partial t}. \tag{17}$$

As we can see from equations (14) and (15), one needs to solve the linear system of equations at each time moment for this implicit scheme. In this case, the computational cost can be expensive, especially for iterative solvers. However, the matrix $\mathbf{A}$ stays unchanged for the constant size of the time step, Δt. Therefore, it is beneficial to adopt the direct solver in order to keep the matrix factorization for the same time step size. We use SuiteSparse v4.5.3 (Davis, 2006) for matrix factorization. In order to speed up the computation, we adopt an adaptive time step doubling method (ATSD) to adjust the step size Δt (Press et al., 1992; Um et al., 2012). Within the framework of this approach, a constant size of the time step, Δt, is kept for n time moments. After that, the time-domain response is calculated at a time of $t + 2\Delta t$ using two different step sizes of Δt and $2\Delta t$, respectively. If the calculated fields from these two different steps are close to each other, the time step doubling is accepted. Otherwise, the original time step, Δt, is used for the following n time moments until the next time step doubling trial is performed. We select $n = 100$ based on our numerical testing.

Before the time stepping, we have to specify the initial conditions for the electric field. The initial condition of zero values of the field should be used for the step-on and impulse-type source waveforms. However, the initial condition of nonzero values can be used for other source waveforms such as the step-off excitation. The FETD modeling of the step-off excitation requires solving a DC problem first to obtain the initial field values and this will be implemented in the future research. In this paper, we use the impulse-type waveform of the source

approximated by Gaussian function to simplify the initial condition. The time domain field caused by other arbitrary source waveform can be obtained by a convolution between the impulse-type response and the actual source waveform (Ward and Hohmann, 1988).

3. Modeling IP effects with adaptive Padé series

Previously, we assumed that the electric conductivity was time and frequency independent. However, we often encounter the frequency-dependent conductivity in geophysical exploration, and this phenomenon is manifested by the IP effect (Ward and Hohmann, 1988; Hallof, 1990; Luo and Zhang, 1998; Seigel et al., 2007; Zhdanov, 2009). There exist different dispersion models to describe the IP phenomenal. Pelton et al. (1978) derived the *Cole-Cole relaxation model* based on the equivalent circuit. As an extension of the Debye model, the *Cole-Cole relaxation model* converges to Debyes, when the relaxation parameter is equal to 1. The *Cole-Cole relaxation model* uses a distribution of the relaxation time values and as a result can take into account a wider dispersion comparing to the Debye model (Tarasov and Titov, 2013). Zhdanov (2008) introduced the generalized effective-medium theory of induced polarization (GEMTIP). The Cole-Cole model can be explained as a reduced form of the GEMTIP model for inclusions having spherical shape. Due to the mathematical simplicity and its ability to explain the commonly encountered IP relaxation, the Cole-Cole model is still widely used (e.g. Marchant et al., 2014).

The Cole-Cole relaxation model of electric conductivity can be described as:

$$\sigma(\omega) = \sigma_0(1 - \eta(1 - \frac{1}{1 + (i\omega\tau)^c}))^{-1}, \tag{18}$$

where σ_0 is the DC conductivity with the unit of S/m, η is the chargeability (unitless), τ is the time parameter with the unit of second (s), and c is the unitless relaxation parameter ranges from 0 to 1.

We consider the Ohm's law in a different form, which relates the electric

field and current density in frequency domain, as follows:

$$\mathbf{E}(\omega) = \rho(\omega)\mathbf{j_e}(\omega) \tag{19}$$

By substituting the Cole-Cole relaxation in equation (18) in equation to (19), we can write the Ohm's law (3) as follows:

$$\sigma_0\mathbf{E}(\omega) + (i\omega)^c\tau^c\sigma_0\mathbf{E}(\omega) = \mathbf{j_e}(\omega) + (i\omega)^c(1-\eta)\tau^c\mathbf{j_e}(\omega) \tag{20}$$

First of all, we consider a simple Debye model with $c = 1$ (Marchant et al., 2014). In this case, equation (20) reduces to the following form:

$$\sigma_0\mathbf{E}(\omega) + (i\omega)\tau\sigma_0\mathbf{E}(\omega) = \mathbf{j_e}(\omega) + (i\omega)(1-\eta)\tau\mathbf{j_e}(\omega) \tag{21}$$

By applying the inverse Fourier transform to (21), we arrive at Ohm's law in the time domain with IP effect:

$$\sigma_0\mathbf{E}(t) + \tau\sigma_0\frac{\partial\mathbf{E}(t)}{\partial t} = \mathbf{j_e}(t) + \tau(1-\eta)\frac{\partial\mathbf{j_e}(t)}{\partial t}, \tag{22}$$

Considering the finite difference scheme in equations (12) and (13), we can write equation (22) as:

$$\sigma_0\mathbf{E}(t) + \frac{\tau\sigma_0}{\Delta t}(\mathbf{E}(t) - \mathbf{E}(t-\Delta)) = \mathbf{j_e}(t) + \frac{\tau(1-\eta)}{\Delta t}(\mathbf{j_e}(t) - \mathbf{j_e}(t-\Delta t)). \tag{23}$$

The simple rearrangement of equation (23) gives the expression of the current density as:

$$\mathbf{j_e}(t) = \frac{(\Delta t+\tau)\sigma_0}{\Delta t+\tau(1-\eta)}\mathbf{E}(t) - \frac{\tau\sigma_0}{\Delta t+\tau(1-\eta)}\mathbf{E}(t-\Delta t) + \frac{\tau(1-\eta)}{\Delta t+\tau(1-\eta)}\mathbf{j_e}(t-\Delta t). \tag{24}$$

Similarly, we can write equation (4) as:

$$\nabla\times\nabla\times\mathbf{E}(t) + \frac{\mu}{\Delta t}\mathbf{j_e}(t) - \frac{\mu}{\Delta t}\mathbf{j_e}(t-\Delta t) = -\mu\frac{\partial\mathbf{J_s}(t)}{\partial t}. \tag{25}$$

By substituting equation (24) into equation (25) and eliminating the term $\mathbf{j_e}(t)$, we obtain:

$$\nabla\times\nabla\times\mathbf{E}(t) + \frac{(\Delta t+\tau)\mu\sigma_0}{\Delta t[\Delta t+\tau(1-\eta)]}\mathbf{E}(t) = \tag{26}$$
$$\frac{\tau\mu\sigma_0}{\Delta t[\Delta t+\tau(1-\eta)]}\mathbf{E}(t-\Delta t) + \frac{\mu}{\Delta t+\tau(1-\eta)}\mathbf{j_e}(t-\Delta t) - \mu\frac{\partial\mathbf{J_s}(t)}{\partial t}.$$

Equation (26) can be used to calculate the electric field, $\mathbf{E}(t)$, in a time stepping manner for Debye relaxation model with the given value of electric field, $\mathbf{E}(t - \Delta t)$, and current density, $\mathbf{j_e}(t - \Delta t)$, at the previous time moment, and with the source waveform. By applying FETD analysis (see section 2), we can solve the system of finite element equations for (26) to obtain the electric field, $\mathbf{E}(t)$. We want to emphasize that in equation (26), the parameter of unknown is the electric field $\mathbf{E}(t)$ at the time moment t. In the finite element system of equation, we only discretize the electric field at the time moment of t and assume that the current density at the previous time steps are already known. Once we solve the electric field at the current moment of t, we can use (24) to calculate the current density at the moment of t.

Note that, in the framework of the FETD method, the electric fields are assigned on the edges of the elements, which automatically enforces continuity of the tangential components of the electric field. At the same time, one cannot use the same approach for the current density, $\mathbf{j_e}$, because the tangential components of the current density are not continuous on the boundary with the conductivity's discontinuity.

In order to solve this problem, we assign the values of the current density at the Gaussian integral points inside of each tetrahedral element. The Gaussian quadrature method is used to calculate the integral of the dot product between edge-based function and the current density in the finite element formulation of the right hand side (RHS) of equation (26). With the known electric field in the Gaussian integral point, we can use (24) to calculate the current density at time moment t. By solving equations (24) and (26) in a recursive manner, we can calculate the electric field directly in the time domain taking into the IP effect, represented by the Debye relaxation model. Note that, equation (24) provides a simple explicit expression for the current density, $\mathbf{j_e}(t)$, at a moment t using the known value of the current density, $\mathbf{j_e}(t - \Delta t)$, at a previous moment, $(t-\Delta t)$.

Next, we consider a general scenario of the Cole-Cole relaxation described by equation (20) with $c \neq 1$. Applying inverse Fourier transform, equation (20) can be transformed into the fractional differential equation (Miller and Ross,

1993; Meerschaert and Tadjeran, 2004):

$$\sigma_0 \mathbf{E}(t) + \tau\sigma_0 \frac{\partial^c \mathbf{E}(t)}{\partial t^c} = \mathbf{j}_\mathbf{e}(t) + \tau(1-\eta)\frac{\partial^c \mathbf{j}_\mathbf{e}(t)}{\partial t^c}. \tag{27}$$

In the last formula, the fractional derivative of real order c is defined as (Caputo, 1967):

$$\frac{\partial^c f(t)}{\partial t^c} = \frac{1}{\Gamma(n-c)} \int_c^t \frac{f^{(n)}(s)ds}{(t-s)^{c-n+1}}, \tag{28}$$

where n is the nearest integer greater than c, $f^{(n)}(s)$ is the n-th order derivative of $f^{(n)}(s)$, and Γ is the gamma function. However, the direct approximation of fractional differential equation is usually avoided, due to its numerical complexity, by using such methods as Laplace transformation (Ge et al., 2012, 2015).

We apply an alternative approach to approximate equation (20) for a dispersive medium, based on expansion of the rational function $(i\omega)^c$ (where $0 < c < 1$) in a form of Padé series (Baker, 1996; Weedon and Rappaport, 1997; Marchant et al., 2014). These series usually converge for rational functions much faster than Taylor series. The Padé approximation of order (M, N) to function $r(x)$ is usually defined as a rational function $R_{M,N}(x)$ expressed in the following form:

$$r(x) \approx R_{M,N}(x) = \frac{P_M(x)}{Q_N(x)}, \tag{29}$$

where $P_M(x)$ and $Q_N(x)$ are two polynomials:

$$P_M(x) = \sum_{m=0}^{M} p_m x^m, \quad Q_N(x) = \sum_{n=0}^{N} q_n x^n. \tag{30}$$

where the parameters m and n are some summation index.

Following Marchant et al. (2014), we approximate the term $(i\omega)^c$ in (20) by the Padé series with $M = N$ and $q_0 = 1$, as follows:

$$(i\omega)^c = \frac{\sum\limits_{m=0}^{M} p_m (i\omega)^m}{1 + \sum\limits_{m=1}^{M} q_m (i\omega)^m}. \tag{31}$$

By substituting equation (31) into equation (20), we obtain the following equation in the frequency domain:

$$a_0\sigma_0\mathbf{E}(\omega)+\left[\sum_{m=1}^{M}a_m(i\omega)^m\right]\sigma_0\mathbf{E}(\omega)=b_0\mathbf{j_e}(\omega)+\left[\sum_{m=1}^{M}b_m(i\omega)^m\right]\mathbf{j_e}(\omega) \quad (32)$$

where we have defined the coefficients a_m and b_m $(m=0,1,....M)$ as:

$$\begin{aligned} a_0 &= 1+P_0(\omega)\tau^c, \\ a_m &= Q_m(\omega)+P_m(\omega)\tau^c, \\ b_0 &= 1+P_0(\omega)(1-\eta)\tau^c, \\ b_m &= Q_m(\omega)+P_m(\omega)(1-\eta)\tau^c. \end{aligned}$$

Note that, the fractional orders disappeared in equation (32) and all the orders are integer numbers now. By applying the inverse Fourier transform to equation (32) we arrive at the following high order ordinary differential equation in the time domain:

$$a_0\sigma_0\mathbf{E}(t)+\sum_{m=1}^{M}\left(a_m\sigma_0\frac{\partial^m\mathbf{E}(t)}{\partial t^m}\right)=b_0\mathbf{j_e}(t)+\sum_{m=1}^{M}\left(b_m\frac{\partial^m\mathbf{j_e}(t)}{\partial t^m}\right). \quad (33)$$

We use the high order backward Euler method for the time discretization (Marchant et al., 2014):

$$\frac{\partial^m f(t)}{\partial t^m}\approx\frac{\sum_{k=0}^{m}(-1)^k\binom{m}{k}f(t-\Delta t)}{\Delta t^m}. \quad (34)$$

By substituting equation (34) into equation (33), we can obtain:

$$\tilde{a}\sigma_0\mathbf{E}(t)+\sum_{m=1}^{M}\left(\frac{a_m}{\Delta t^m}\sigma_0\mathbf{E}^m\right)=\tilde{b}\mathbf{j_e}(t)+\sum_{m=1}^{M}\left(\frac{b_m}{\Delta t^m}\mathbf{j_e}^m\right), \quad (35)$$

where we have introduced the auxiliary parameters:

$$\begin{aligned} \tilde{a} &= \sum_{m=0}^{M}\frac{a_m}{\Delta t^m}, \\ \tilde{b} &= \sum_{m=0}^{M}\frac{b_m}{\Delta t^m}, \end{aligned}$$

$$\mathbf{E}^m = \sum_{k=1}^{m} (-1)^k \binom{m}{k} \mathbf{E}(t - \Delta t),$$
$$\mathbf{j_e}^m = \sum_{k=1}^{m} (-1)^k \binom{m}{k} \mathbf{j_e}(t - \Delta t).$$

We need to note that this numerical scheme works well even when we use the ATSD method to increase the time step size from Δt to $2\Delta t$ at the time moment of t. We never use a mixed time step size in these equations. When the time step size is changed to $2\Delta t$, the parameter of Δt in the previous equations are all replaced by $2\Delta t$. As a result, the solution of electric fields at previous steps of $t - 2\Delta t$, $t - 4\Delta t$, etc., which has already been computed using the old time step size of Δt, is needed.

From equation (35), we can derive the explicit equation for the current density $\mathbf{j_e}(t)$:

$$\mathbf{j_e}(t) = \frac{\tilde{a}}{\tilde{b}} \sigma_0 \mathbf{E}(t) + \sum_{m=1}^{M} \left(\frac{a_m}{\tilde{b} \Delta t^m} \sigma_0 \mathbf{E}^m \right) - \sum_{m=1}^{M} \left(\frac{b_m}{\tilde{b} \Delta t^m} \mathbf{j_e}^m \right). \tag{36}$$

Similar as was done for the case of Debye relaxation model, we can substitute equation (36) into equation (25), and arrive at:

$$\nabla \times \nabla \times \mathbf{E}(t) + \frac{\mu \tilde{a}}{\Delta t \tilde{b}} \sigma_0 \mathbf{E}(t) = \tag{37}$$
$$\frac{\mu}{\Delta t} \mathbf{j_e}(t - \Delta t) - \mu \frac{\partial \mathbf{J_s}(t)}{\partial t} - \sum_{m=1}^{M} \left(\frac{\mu a_m}{\tilde{b} \Delta t^{m+1}} \sigma_0 \mathbf{E}^m \right) + \sum_{m=1}^{M} \left(\frac{\mu b_m}{\tilde{b} \Delta t^{m+1}} \mathbf{j_e}^m \right).$$

By applying the edge-based finite-element method with linear basis functions to equation (37), we obtain:

$$K\mathbf{E}(t) + \frac{\mu \tilde{a}}{\Delta t \tilde{b}} L_0 \mathbf{E}(t) = \frac{\mu}{\Delta t} \int_{V_e} \mathbf{N}_i^e \cdot \mathbf{j_e}(t - \Delta t) dv - \mu \int_{V_e} \mathbf{N}_i^e \cdot \frac{\partial \mathbf{J_s}(t)}{\partial t} dv$$
$$- \sum_{m=1}^{M} \left(\frac{\mu a_m}{\tilde{b} \Delta t^{m+1}} L_0 \mathbf{E}^m \right) + \int_{V_e} \mathbf{N}_i^e \cdot \left[\sum_{m=1}^{M} \left(\frac{\mu b_m}{\tilde{b} \Delta t^{m+1}} \mathbf{j_e}^m \right) \right] dv. \tag{38}$$

where the stiffness matrix L_0 is similar as L which is defined in equation (10), but for DC conductivity σ_0

After solving equation (38) to find the electric field, we apply equation (36) to calculate the current density $\mathbf{j_e}(t)$.

From the derivations, one can see that the accuracy of our modeling depends on how accurately we can approximate the $(i\omega)^c$ term using the Padé series as shown in equations (29) and (31). As in the case of the Taylor series expansions, the accuracy of the Padé series for the $(i\omega)^c$ term is only guaranteed in the vicinity of the frequency, ω_0, at which the Padé expansion is performed:

$$(i\omega)^c = (i\omega_0)^c + \frac{\sum_{m=0}^{M} p_m \left[i\left(\omega-\omega_0\right)\right]^m}{1+\sum_{m=1}^{M} q_m \left[i\left(\omega-\omega_0\right)\right]^m}. \tag{39}$$

Here, ω_0 is the center angular frequency for Padé series, and f_0 is the corresponding center frequency:

$$f_0 = \frac{\omega_0}{2\pi}. \tag{40}$$

Note that, for Debye model, $c = 1$, the term of $(i\omega)$ can be perfectly represented by the Padé series for any choice of the center frequency.

As an example, we consider a Cole-Cole model with $\sigma_0 = 0.001$ S/m, $\tau = 1$ s, $\eta = 0.1$. First, we consider the Debye relaxation. Fig. 1 shows a comparison between the actual conductivity spectrum and its first order Padé approximation with the center frequency of 1 Hz. The Padé series with other orders and center frequencies produce exactly the same result as the Debye model.

We consider now $c = 0.6$, and use the third order Padé series with different center frequencies to approximate the actual conductivity spectrum. Two center frequencies with the values of 0.01 Hz and 100 Hz were used. Fig. 2 presents a comparison between the Cole-Cole conductivity spectrum and the corresponding Padé approximations with these two different center frequencies. One can see that the low frequency part of the spectrum is well fitted by the Padé approximation with the center frequency of $f_0 = 0.01$ Hz; however, the high frequency part shows a clear discrepancy. For the center frequency of $f_0 = 100$ Hz, the high frequency section of the spectrum can be accurately approximated by the Padé series, but not the low frequency part.

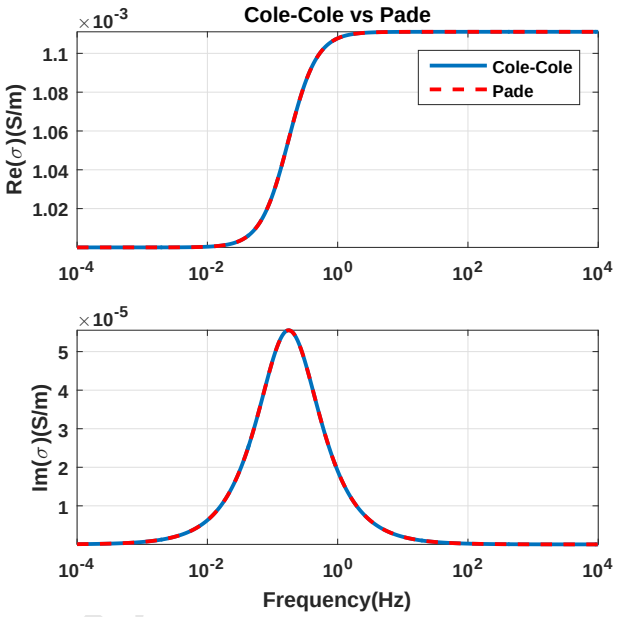

Fig. 1. A comparison between the Cole-Cole conductivity spectrum, for Debye relaxation model, and the corresponding Padé approximation.

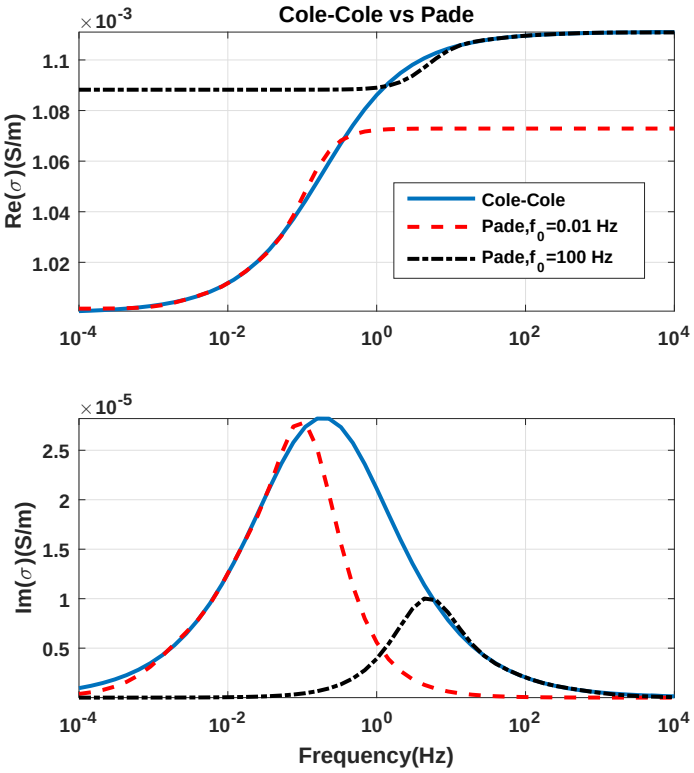

Fig. 2. A comparison between the Cole-Cole conductivity spectrum, with $c = 0.6$, and the corresponding Padé approximation with two different center frequencies.

For the same center frequency, the accuracy of the Padé approximation can be improved by adopting higher order Padé approximation. However, the higher-order Padé series can result in instability problems. In our modeling, the order of Padé approximation is selected automatically by the algorithm. It starts with lower order and only increase the order when the IP spectrum cannot be fitted by the lower order Padé approximation. One can see the term, $\Delta t^{-(m+1)}$, for the Padé series of order m in equation (38). Based on our experience, the time step, Δt, could be as small as 10^{-6} s in order to accurately represent the impulse waveform and produce an accurate early time response. For such small time step, the term $\Delta t^{-(m+1)}$ can become extremely large for high order Padé series, which can cause serious numerical problems (Ascher and Greif, 2011).

In order to avoid the use of high order Padé series, it is crucial to select the proper center frequency for Padé series. We introduce an adaptive method of selecting the center frequency for Padé series. The key idea of the adaptive Padé series is based on using the large center frequency in early time and gradually decreasing the center frequency with the increase of time moments.

We divide the total observation time period into a series of segments and the time step sizes for FETD modeling within each segment are the same. For a model with Cole-Cole relaxation, the true time domain response of a half-space model, with the same relaxation model, is calculated by cosine transform for each time segment. The corresponding Padé approximation for the same time segment is also calculated for a series of trial center frequencies. A large frequency range with fine frequency sampling will be better. However, we find that the frequency range between 10^{-3} Hz to 10^{3} Hz with 5 frequency per decade (in logarithmic space) is good enough to ensure the modeling accuracy. The optimal center frequency is selected, for each time segment, based on the misfit between the Padé approximation and the true half-space response. Comparing to the method which use one center frequency for the entire time period (Marchant et al., 2014), we found that the adaptive method produces a better result for Padé series with the relatively lower order. For a 3D model with variable relaxation

```
Define parameters:
t=0: initial time
Δt0: initial time step size
t_max: time period for the modeling

Main Code:
for it=1:MaxIteration
        Δt=Δt0
        t=t+Δt
        if t>=t_max
            break;
        end

        if it=1
            Get optimized Padé series expansion
        end

        Do FETD modeling with the obtained Padé series and time step size

        if it can be divided by 100
            Do ATSD (automatic time step doubling)
            Recompute the optimized Padé series
        End

        Continue FETD modeling with the updated Padé series and time step size

end
```

Fig. 3. Pseudocode for the described FETD modeling algorithm with adaptive Padé approximation.

parameter, of c, an equivalent half space model with averaged c will be used for Padé approximation. In our future research, we will consider a more strict way to deal with this problem by using different Padé approximation for different area with variable relaxation parameter of c. The described algorithm can be summarized in the pseudocode showing in Fig. 3

To illustrate this approach, we consider again a dispersive half-space model with the Cole-Cole model parameters the same as above: $\sigma_0 = 0.001$ S/m, $\tau = 1$ s, $\eta = 0.1$, $c = 0.6$. The EM field is excited by a horizontal electric ground wire with an impulse moment of 10^5 Am. We first calculated the in-line electric field, E_x, at the offset of 1000 m using cosine transform method for the actual

model. Next, we calculated the same E_x field using the Padé approximation with both optimized fixed center frequency and using the adaptive selection for the center frequency. Fig. 4 presents a comparison between E_x produced using the actual model and the Padé approximation with both fixed and adaptive center frequency.

We can see that the adaptive Padé approximation produces almost the same time domain response as the true model. However, the response computed using the Padé approximation with fixed center frequency shows some difference comparing to the response for the actual model (especially near $t = 10^{-2}$ s). In order to better demonstrate these results, we have normalized the time domain responses produced by the Padé approximation with adaptive and fixed center frequencies by the time domain response for the actual half-space model. The calculated rations are presented in Fig. 5. One can clearly see the advantage of the adaptive Padé method over the Padé series with a fixed center frequency.

Fig. 6 presents a plot of the center frequency for the adaptive Padé method as a function of time. We can see that the center frequency decreases with time, which reflects well the fact that the late time response corresponds to the low frequency signal. For the Padé approximation with the fixed frequency, the optimized center frequency was 0.4 Hz.

4. Model Studies

We now demonstrate the developed algorithm using several model studies. At first, we consider a half space model with IP effect for both Debye and a general Cole-Cole conductivity relaxation. Then, we consider a model with non-dispersive half-space background and localized dispersive 3D anomaly.

4.1. Half space model

Let us consider a half space model with a conductivity of 10^{-3} S/m. The EM field is excited by an $x-$oriented grounded electric bipole source with the center located at $(-1000, 0, 0)$ m and a length of 10 m. An unit impulse electric

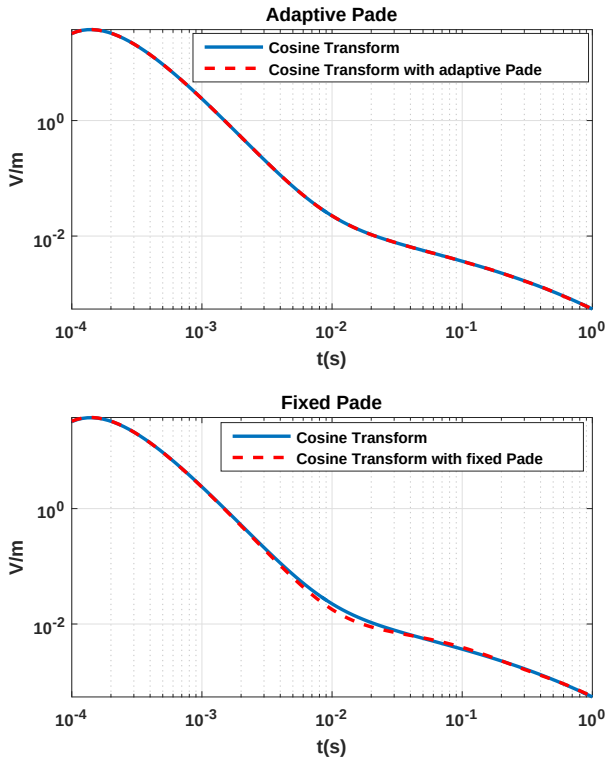

Fig. 4. A comparison between the time domain electric field, E_x, produced using the actual model and the Padé approximation with both adaptive (upper panel) and fixed (lower panel) center frequency. In each panel, the solid blue curve represents the time domain response for the actual half-space model, obtained from cosine transform method.

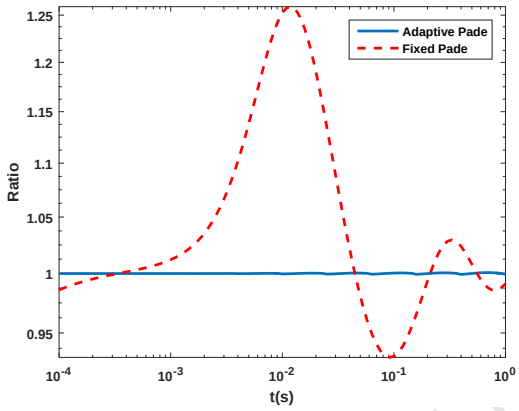

Fig. 5. A comparison between the time domain response computed using the Padé approximation with adaptive (solid blue) and fixed (dashed red) center frequencies. Both responses are normalized by the response for the actual half-space model. A ratio value of 1 indicates that the Padé approximation produces the same result as the true Cole-Cole model.

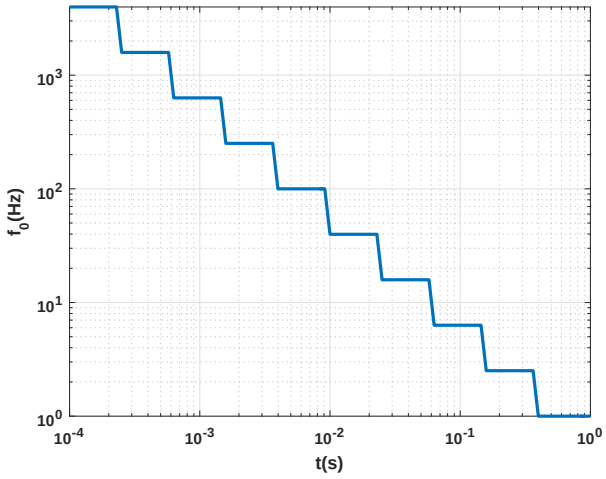

Fig. 6. A plot of the center frequency for the adaptive Padé method as a function of time for the half-space model.

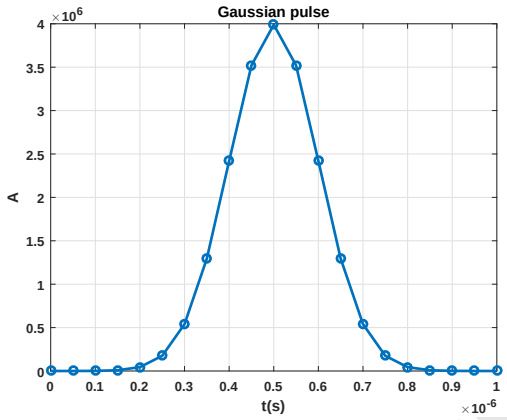

Fig. 7. Discretization of the Gaussian pulse waveform.

current is injected into the bipole. The inline electric field, E_x, will be recorded at two offsets of 1000 m and 2000 m from the bipole.

The time constant τ is set to 1 s and the chargeability η is set to be 0.1. For comparison, the time domain response is also calculated by the frequency-time domain transformation (Ward and Hohmann, 1988). For all models in this paper, we use 51 frequencies uniformly spaced in logarithmic space from 10^{-5} Hz to 10^5 Hz to perform the frequency-time domain transformation.

We approximate the impulse signal with a Gaussian pulse (Jin, 2014). A short duration time for the Gaussian pulse is required to accurately approximate the impulse. Fig. 7 shows the discretization of the Gaussian pulse used for this model which results in an initial time step size of 5×10^{-8} s. Note that the maximum current in Fig. 7 is 4×10^6 Ampere since the integral of current over time for this Gaussian impulse is equal to 1 which is equivalent to the unit impulse electric current source.

The modeling domain was selected to be 80 km $\times$ 80 km $\times$ 80 km in the x, y, and z directions. The domain was discretized using unstructured tetrahedral mesh, which contains $162,394$ elements and $193,341$ edges. The resulting size of the finite element system of equations was $193,341 \times 193,341$.

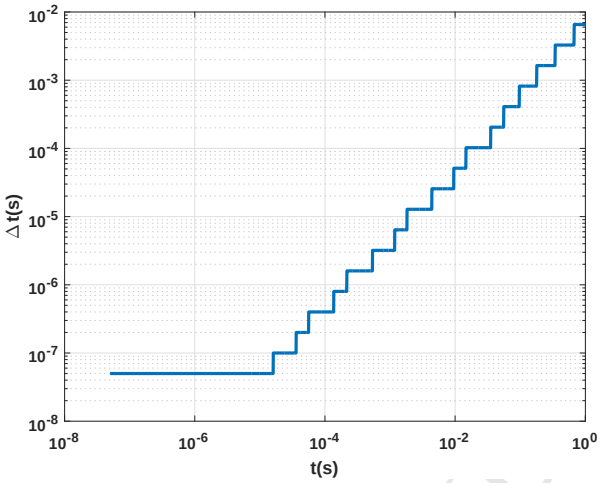

Fig. 8. A plot illustrating the increase of the time step size with time for the half-space model with no IP effect.

4.2. Debye dispersion

First, we consider the Debye relaxation model with $c = 1$. In this case, there is no need to use the Padé approximation because the FETD method can be applied directly to solving equation (26).

We calculated the time domain response up to late time of $t = 1$ s. It only took 6 minutes to complete the calculation with 2671 time steps. Note that the number of time steps would be 20 million without adopting the ATSD scheme. Fig. 8 shows an increase of the size of time steps with time for this model.

The upper and lower panels of Fig. 9 show the comparisons between the FETD modeling results and the analytical solutions for this model at the offset of 1000 m and 2000 m, respectively. We can see that the FETD results compare well to the analytical solutions. Fig. 10 shows a comparison between the electric field for the non-dispersive half space model and the half space model with Debye dispersion at the vertical plane of $y = 300$ m. We can clearly see that the time domain response is distorted significantly by the IP effect.

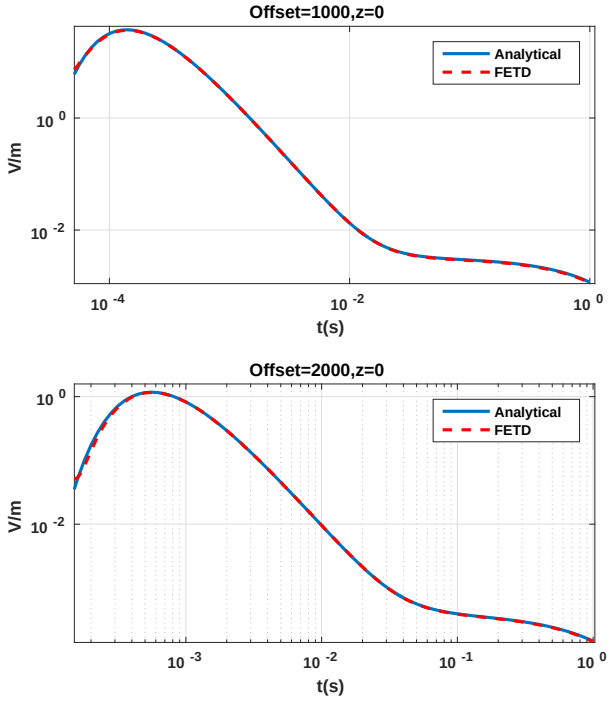

Fig. 9. A comparison between the analytical solution and FETD solution at the offset of 1000 m (upper panel) and 2000 m (lower panel) for the half-space model with Debye dispersion.

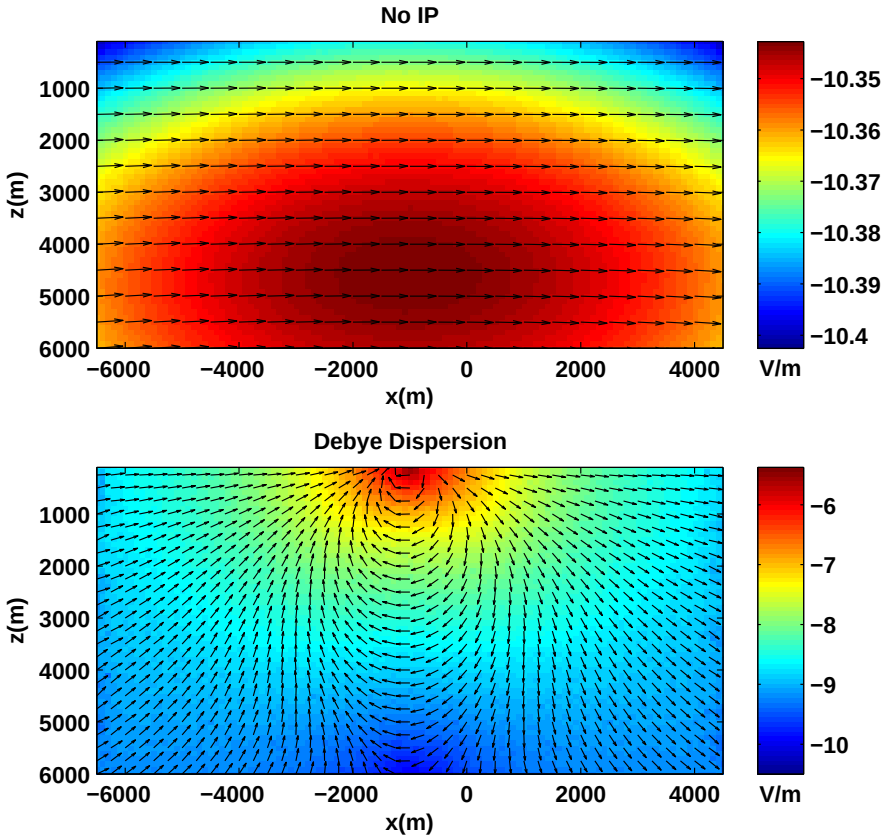

Fig. 10. A comparison between the time domain electric field for the non-dispersive half-space model (upper panel) and half-space model with Debye type dispersion (lower panel), at $y = 300$ m and $t = 0.22$ s. The arrow represents the direction of the total electric field on this vertical plane. The colorbar uses a logarithmic scale.

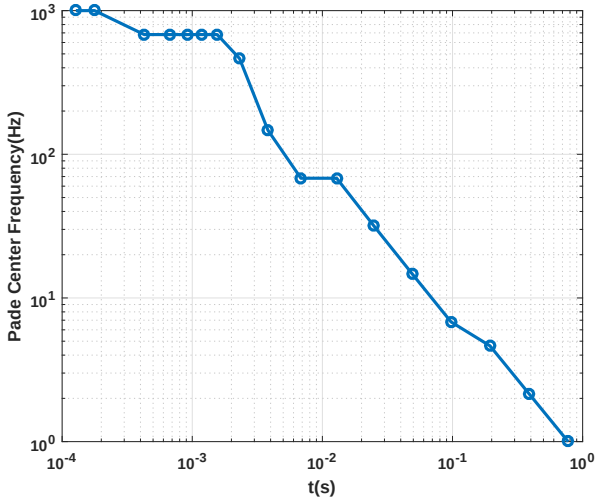

Fig. 11. A plot of the center frequency for the adaptive Padé method as a function of time for the Cole-Cole conductivity relaxation model of the half space with $c = 0.6$.

4.3. Cole-Cole dispersion

We now consider a general Cole-Cole conductivity relaxation with $c \neq 1$. At first, we consider $c = 0.6$. We use the Padé series with the order of three to approximate the Cole-Cole model and the center frequency of the Padé series is selected in an adaptive manner. Fig. 11 shows the optimized Padé series center frequency used for the FETD modeling at different time stages. The value of the center frequency decreases with time increase, as we have expected.

The upper and lower panels of Fig. 12 show the FETD modeling results for this half-space dispersion model, with $c = 0.6$, compared to the analytical solutions at two different offsets. We can clearly see that the FETD solutions corresponds well to the analytical solution for both early and late time.

We now consider another case of $c = 0.4$ for this half-space model. Fig. 13 shows a comparison between the FETD and the corresponding analytical solutions. We can see that the FETD solution still compares well with the analytical solution. A smaller value of c corresponds to a broader dispersion spectrum, which is more difficult to describe by the Padé series with order 3.

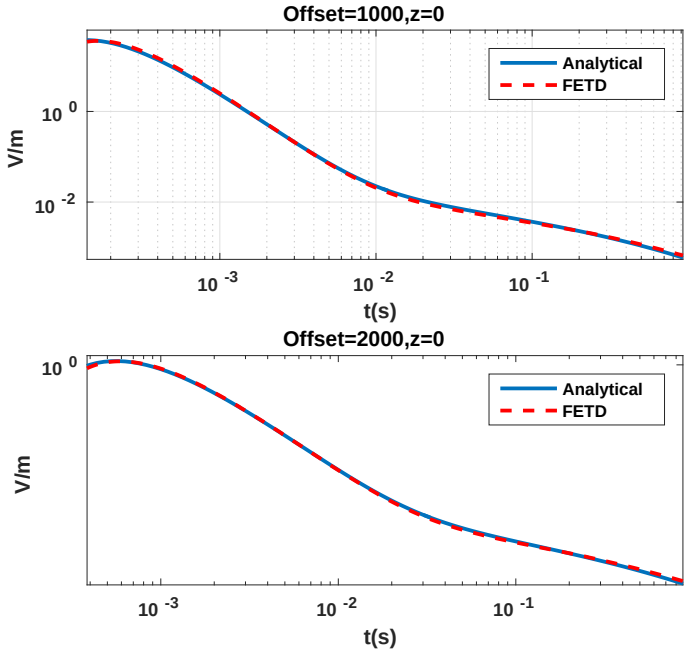

Fig. 12. A comparison between the analytical and FETD solutions at the offset of 1000 m (upper panel) and 2000 m (lower panel) for the Cole-Cole dispersive half-space model with $c = 0.6$.

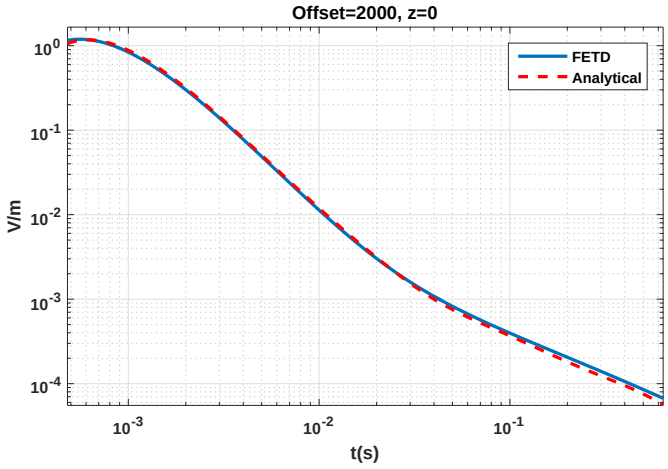

Fig. 13. A comparison between the analytical and FETD solutions at the offset of 2000 m for the Cole-Cole dispersive half-space model with $c = 0.4$.

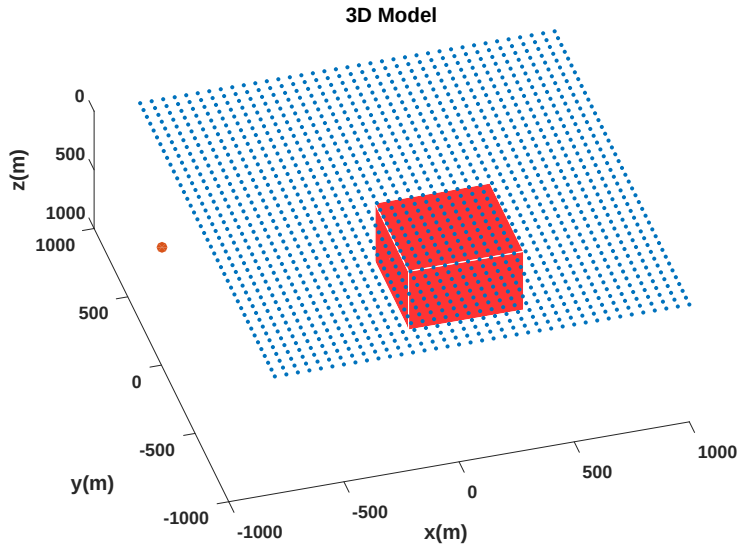

Fig. 14. A 3D model of a conductive cube located within a homogeneous half space. The blue dots represent the receiver locations, while the red dot on the left indicates the center position of the electric bipole source.

4.4. 3D model

Now, we consider a 3D model shown in Fig. 14. The source is exactly the same as in the previous section. This model consists of a half space background with the conductivity of 10^{-3} S/m, and a cubic anomaly with the conductivity of 10^{-2} S/m. The size of the cube is 500 m $\times$ 500 m $\times$ 500 m, its center is located at a point with coordinates of $(0, 0, 500)$ m. The size of the modeling domain was 80 km $\times$ 80 km $\times$ 80 km. The tetrahedral discretization of this domain contained $270,553$ elements and $319,029$ edges.

For comparison, we also calculated the frequency domain response using the frequency-domain FEM code (Cai et al., 2017), and the cosine transformation was applied to calculate the time-domain response.

In the first numerical test we assumed that there was no IP effect. Fig. 15 shows a comparison between the FETD solution and the frequency domain transformed solution, at $t = 0.1$ s, on the earth's surface. Fig. 16 shows a

similar comparison at the receiver located directly above the center of the 3D body. We can see that the FETD solution compares well with the frequency domain transformed solution. The total computation time for this model was only 10 minutes, with 1416 time steps.

In the next example, we consider the same 3D model, but with the dispersive conductivity of the cubic body. We first consider a simple Debye relaxation model for anomalous conductivity with $\tau = 0.1$ s and $\eta = 0.5$.

Fig. 17 shows a comparison between the FETD solution and the frequency domain transformed solution, at $t = 0.1$ s for this dispersive model. We can see that the FETD solution compares well with the frequency domain transformed result. By comparing this figure with Fig. 15, one can clearly see that the field is distorted significantly by the IP effect.

Fig. 18 shows the time domain response, obtained from FETD and cosine transformation, for this 3D IP model with Debye dispersion at the receiver which is directly above the center of the 3D body. The total computation time is around 15 minutes after 1416 time steps. We can see that the computation complexity increases after considering the IP effect.

Finally, we consider a general case of the Cole-Cole model with $c = 0.6$,. The optimized Padé series with third order and adaptive center frequency were applied. Fig. 19 shows the center frequency of the adaptive Padé series expansion at different time stages.

Fig. 20 shows a comparison between the FETD solution and the frequency domain transformed result for this model at $t = 0.1$ s, on the earth's surface. Fig. 21 presents the FETD solution and the frequency domain transformed solution at different time stage for the receiver directly above the center of the 3D body. From these figures, we can see that the FETD solution compares well with the frequency-domain transformed result. The computation time was around 27 minutes after 1416 time steps. For all the above scenarios of this 3D model, the run time for the frequency-domain finite element code was around 3 hours in the same machine and we have used 51 frequencies uniformly spaced in logarithmic space from 10^{-5} Hz to 10^{5} Hz. We want to emphasize that the

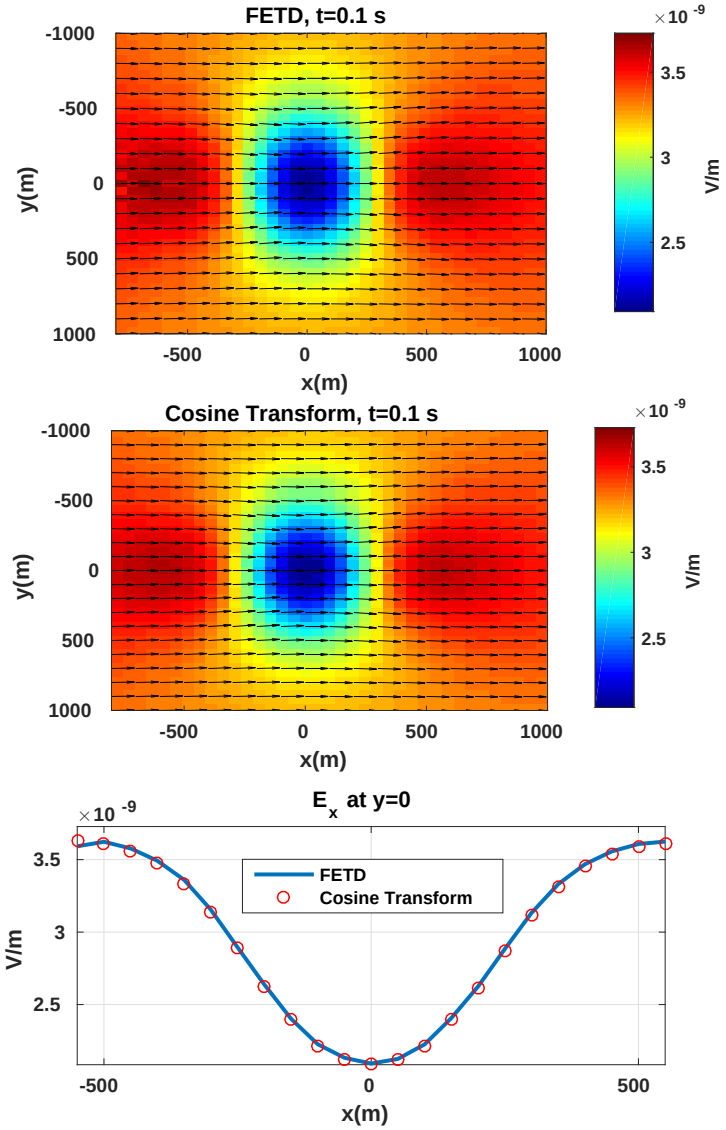

Fig. 15. A comparison between the FETD solution and the frequency domain transformed solution for the 3D model with no IP effect. The upper and middle panel shows the map view on the earth's surface where the arrows represent the direction of the electric field on the earth's surface. The lower panel shows a comparison at $y = 0$ on the earth's surface.

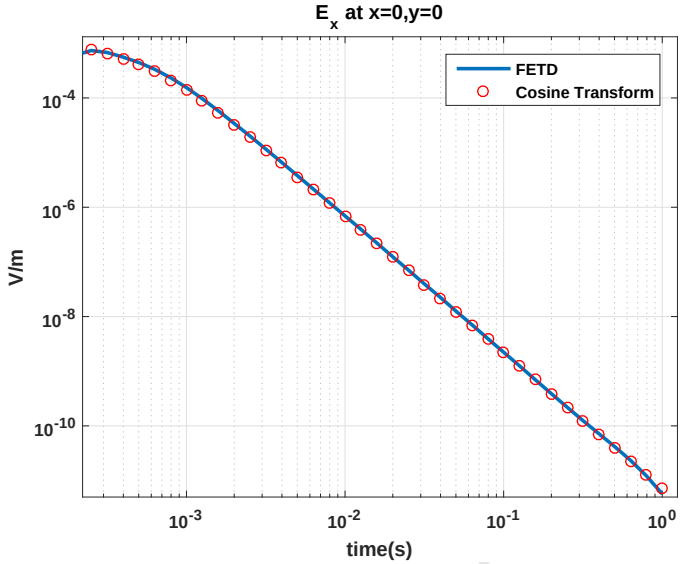

Fig. 16. A comparison between the FETD solution and the frequency domain transformed solution for the 3D model with no IP effect in the receiver located directly above the center of the anomaly.

solver for our FETD algorithm is only serial version but the frequency-domain finite element code we used here adopts the Intel MKL Pardiso solver which is fully parallelized.

Finally, for comparison, Fig. 22 presents the plots of the electric field computed for the receiver located directly above the 3D body for four different scenarios: 1) half-space model with no IP effect; 2) 3D conductivity anomaly with no IP effect; 3) 3D conductivity anomaly with Debye relaxation; 4) 3D conductivity anomaly with Cole-Cole relaxation ($c = 0.6$). By comparing the electric field for the homogeneous half-space background model and for a model with 3D anomaly with no IP effect, we can see that the curves are shifted. For both Debye and Cole-Cole models of 3D anomalous conductivity, the IP effect delays the decay of the signal in comparison to the 3D model with no IP effect.

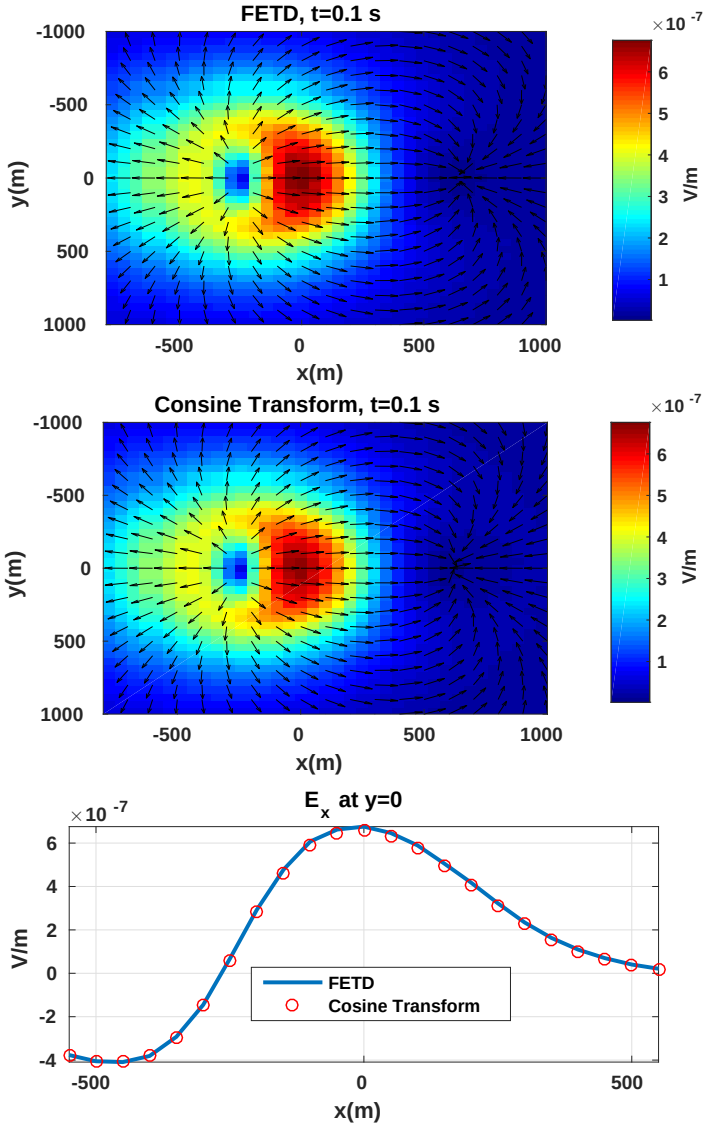

Fig. 17. A comparison between the FETD solution and the frequency domain transformed solution for the 3D model with IP effect described by Debye relaxation model. The upper and middle panel shows the map view on the earth's surface where the arrows represent the direction of the electric field on the earth's surface. The lower panel shows a comparison at $y = 0$ on the earth's surface.

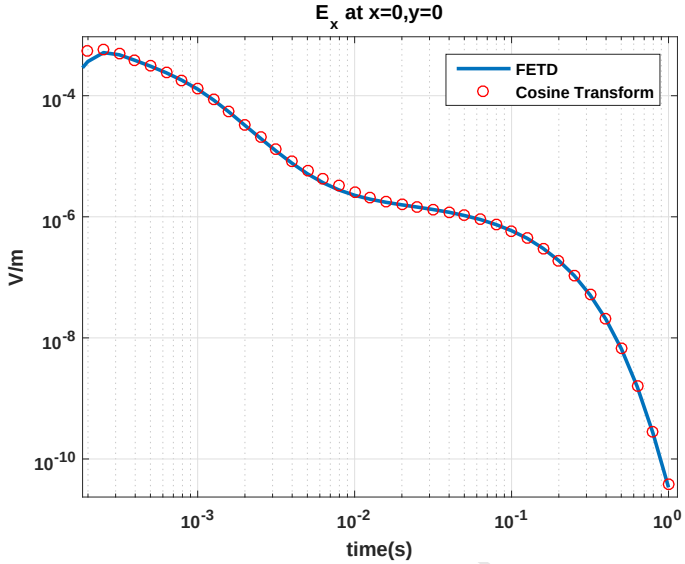

Fig. 18. A comparison between the FETD solution and the frequency domain transformed solution for the 3D model with IP effect described by Debye relaxation model at the receiver located directly above the center of the anomaly.

5. Conclusions

We have developed an edge-based finite-element time-domain method for simulating electromagnetic fields in conductive and dispersive medium. We consider a total field formulation and use unstructured tetrahedral mesh to reduce the size of the problem. We also use the backward difference, which is unconditionally stable, for time domain discretization. We adopt time step doubling methods to gradually increase the step size and reduce the computational expense. The sparse system of equations is solved using the direct method based on a sparse LU decomposition. We have demonstrated that this step doubling method with direct solver can significantly reduce computation time.

The developed FETD modeling method takes into account the conductivity dispersion (IP effect) directly in the time domain. We use the Padé series to approximate the Cole-Cole model, which allows us to approximate the differential equation in the time domain with fractional derivatives by the differential

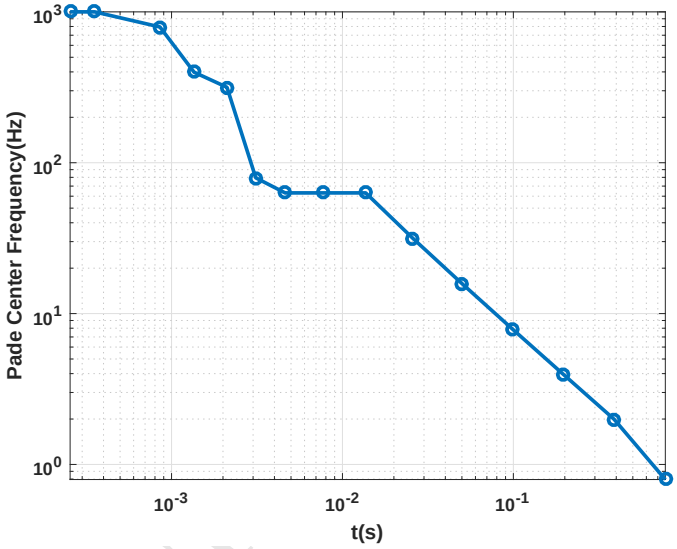

Fig. 19. A plot of the center frequency for the adaptive Padé method as a function of time for the Cole-Cole conductivity relaxation model of 3D anomalous cubic body with $c = 0.6$.

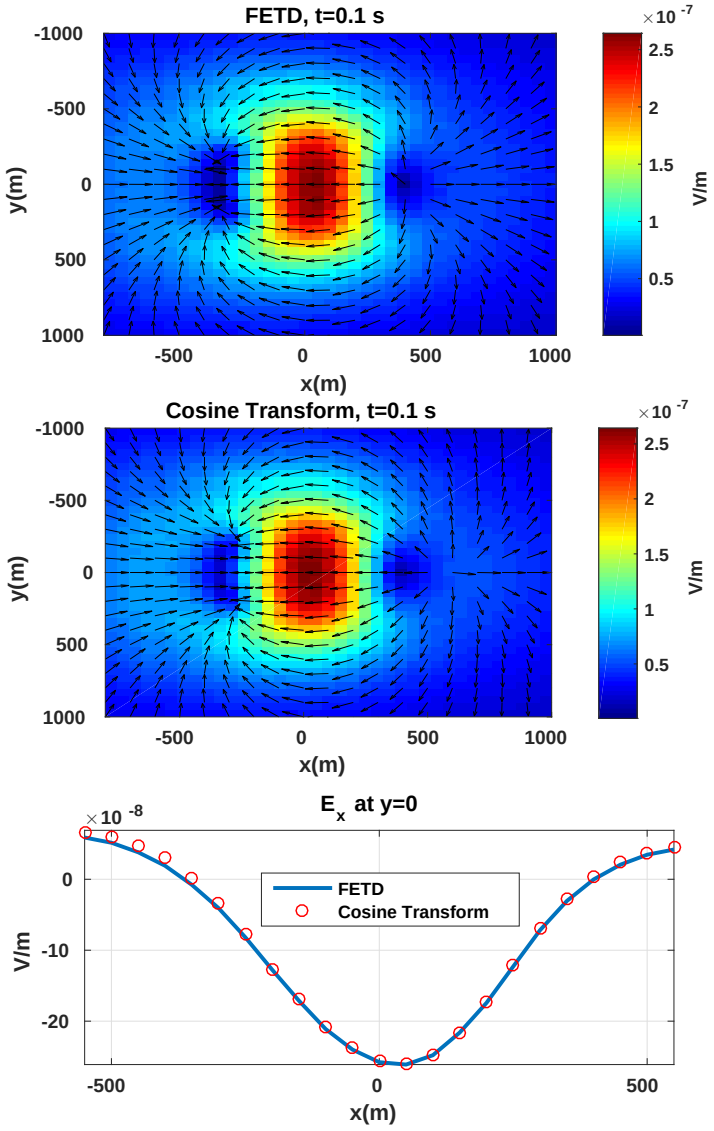

Fig. 20. A comparison between the FETD solution and the frequency domain transformed solution for the 3D model with IP effect described by Cole-Cole relaxation model. The upper and middle panel shows the map view on the earth's surface where the arrows represent the direction of the electric field on the earth's surface. The lower panel shows a comparison at $y = 0$ on the earth's surface.

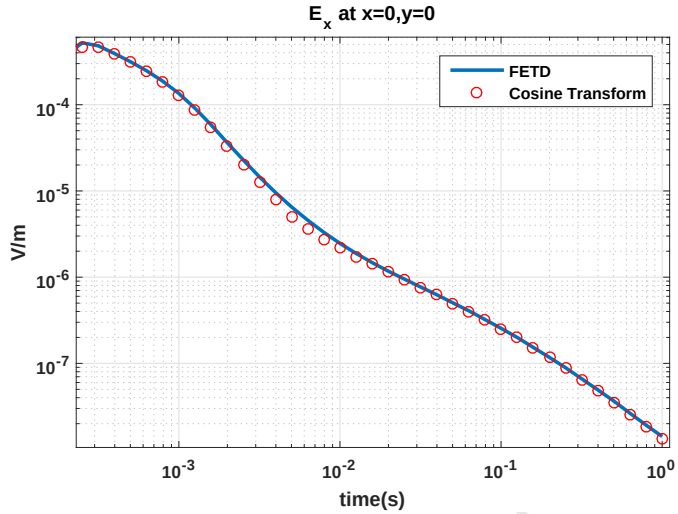

Fig. 21. A comparison between the FETD solution and the frequency domain transformed solution for the 3D model with IP effect described by Cole-Cole relaxation model at in the receiver located directly above the center of the anomaly.

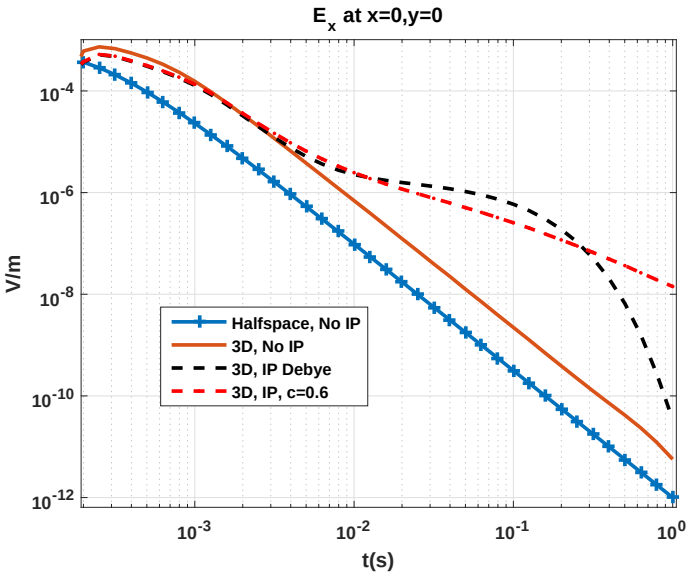

Fig. 22. The plots of the electric field computed for the receiver located directly above the 3D body for four different scenarios.

equation with integer order. In order to increase the accuracy of the Padé approximation for a wide time range, we introduced a method of adaptive Padé series with variable center frequency of the series for early and late time. This approach increases the accuracy of FETD modeling. We validate the developed algorithm using several models with and without the IP effect.

6. Acknowledgement

The authors are thankful to the anonymous reviewers for their valuable suggestions.

References

Ascher U. M. and Greif C., 2011. *A first course in numerical methods*, SIAM, Philadelphia.

Baker, G.A. and Graves-Morris, P.R., 1996. *Padé approximants*, Cambridge University Press, New York.

Cai, H., Hu, X., Li, J., Endo, M. and Xiong, B., 2017. Parallelized 3D CSEM modeling using edge-based finite element with total field formulation and unstructured mesh, *Computers & Geosciences*, **99**, 125-134.

Caputo, M., 1967. Linear model of dissipation whose Q is almost frequency independent-II, *Geophysical Journal Royal Astronomical Society*, **13**, 529–539.

Commer, M. and Newman, G., 2004. A parallel finite-difference approach for 3D transient electromagnetic modeling with galvanic sources, *Geophysics*, **69**, 1192-1202.

Davis, T., 2006. *Direct methods for sparse linear systems*, SIAM, Philadelphia.

Everett, M.E. and Edwards, R.N., 1993. Transient marine electromagnetics: The 2.5-D forward problem, *Geophys. J. Int.*, **113**, 545-561.

Ge, J., Everett, M.E. and Weiss, C.J., 2012. Fractional diffusion analysis of the electromagnetic field in fractured media Part I: 2D approach, *Geophysics*, **77**, WB213-WB218.

Ge, J., Everett, M.E. and Weiss, C.J., 2015. Fractional diffusion analysis of the electromagnetic field in fractured mediaPart 2: 3D approach, *Geophysics*, **80**, E175-E185.

Hallof, P.G. and Yamashita, M., 1990. *Induced polarization applications and case histories*, SEG, Tulsa.

Jin, J., 2014. *Finite element method in electromagnetics, Third Edition*, Wiley-IEEE Press, New York.

Knight, J.H., Raiche, A.P., 1982. Transient electromagnetic calculations using the Gaver-Stehfest inverse Laplace transform method, *Geophysics*, **47**, 47-50.

Li, J., Farquharson, C.G. and Hu, X., 2016. Three effective inverse Laplace transform algorithms for computing time-domain electromagnetic responses, *Geophysics*, **81**, E113-E128.

Luo, Y. and Zhang, G., 1998. *Theory and application of spectral induced polarization*, SEG, Tulsa.

Maaø, F.A., 2007. Fast finite-difference time-domain modeling for marine-subsurface electromagnetic problems, *Geophysics*, **72**, A19-A23.

Marchant, D., Haber, E. and Oldenburg, D.W., 2014. Three-dimensional modeling of IP effects in time-domain electromagnetic data, *Geophysics*, **79**, E303-E314.

Meerschaert, M.M. and Tadjeran, C., 2004. Finite difference approximations for fractional advectiondispersion flow equations, *Journal of Computational and Applied Mathematics*, **172**, 65-77.

Miller, K.S. and Ross, B., 1993. *An introduction to the fractional calculus and fractional differential equations*, Wiley-Blackwell,New York.

Mulder, W.A., Wirianto, M. and Slob, E.C., 2007. Time-domain modeling of electromagnetic diffusion with a frequency-domain code, *Geophysics*, **73**, F1-F8.

Pelton, W.H., Ward, S.H., Hallof, P.G., Sill, W.R. and Nelson, P.H., 1978. Mineral discrimination and removal of inductive coupling with multifrequency IP, *Geophysics*, **43**, 588-609.

Press, W.H., Teukolsky, S.A., Vetterling, W.T. and Flannery, B.P., 1992. *Numerical Recipes in C: The Art of Scientific Computing, Second Edition*, Cambridge University Press.

Raiche, A., 1998. Modelling the time-domain response of AEM systems, *Exploration Geophysics*, **29**, 103-106.

Ralph-Uwe, B., Ernst, O.G. and Spitzer, K., 2008. Fast 3-D simulation of transient electromagnetic fields by model reduction in the frequency domain using Krylov subspace projection, *Geophys. J. Int.*, **173**, 766-780.

Rekanos, I.T. and Papadopoulos, T.G., 2010. An auxiliary differential equation method for FDTD modeling of wave propagation in Cole-Cole dispersive media, *IEEE Transactions on Antennas and Propagation*, **58**, 3666-3674.

Seigel, H., Nabighian, M., Parasnis, D.S. and Vozoff, K., 2007. The early history of the induced polarization method, *The Leading Edge*, **26**, 312-321.

Tarasov, A. and Titov, K., 2013. On the use of the ColeCole equations in spectral induced polarization, *Geophys. J. Int.*, **195**, 352-356.

Um, E.S., 2011. *Three-dimensional finite-element time-domain modeling of the marine controlled-source electromagnetic method*, Ph.D dissertation, Stanford University.

Um, E.S., Harris, J.M. and Alumbaugh, D.L., 2012. An iterative finite element time-domain method for simulating three-dimensional electromagnetic diffusion in earth, *Geophys. J. Int.*, **190**, 871-886.

Wang, T. and Hohmann, G.W., 1993. A finite-difference, time-domain solution for three-dimensional electromagnetic modeling, *Geophysics*, **58**, 797-809.

Ward, S.H., Hohmann, G.W., 1988. *Electromagnetic Theory for Geophysical Applications*, SEG, Tulsa.

Weedon, W.H. and Rappaport, C.M., 1997.A general method for FDTD modeling of wave propagation in arbitrary frequency-dispersive media, *IEEE Transactions on Antennas and Propagation*, **45**, 401-410.

Yee, K.S., 1966. Numerical solution of initial value problems involving Maxwell's equationsin isotropic media, *IEEE Transactions on Antennas and Propagation*, **14**, 302-307.

Zaslavsky, M., Druskin, V. and Knizhnerman, L., 2011. Solution of 3D time-domain electromagnetic problems using optimal subspace projection, *Geophysics*, **76**, F339-F351.

Zhdanov, M., 2008. Generalized effective-medium theory of induced polarization, *Geophysics*, **73**, F197-F211.

Zhdanov, M.S., 2009. *Geophysical electromagnetic theory and methods*, Elsevier, Amsterdam.

This paper develops a finite element time domain algorithm for geophysical application

We consider a frequency dependent conductivity using Cole-Cole relaxation model

The frequency domain relaxation model is transformed into time domain

We propose the adaptive Padé series to approximate the time domain Cole-Cole relaxation